THE JOURNAL OF PHYSICAL CHEMISTRY LETTERS
A JOURNAL OF THE AMERICAN CHEMICAL SOCIETY

pubs.acs.org/JPCL

Letter

Unravelling the Structural Organization of Individual α-Synuclein Oligomers Grown in the Presence of Phospholipids

Tianyi Dou, Lei Zhou, and Dmitry Kurouski*

Cite This: J. Phys. Chem. Lett. 2021, 12, 4407−4414

Read Online

ACCESS | Metrics & More | Article Recommendations | Supporting Information

ABSTRACT: Parkinson's disease (PD) is a severe neurological disorder that affects more than 1 million people in the U.S. alone. A hallmark of PD is the formation of intracellular α-synuclein (α-Syn) protein aggregates called Lewy bodies (LBs). Although this protein does not have a particular localization in the central neural system, α-Syn aggregates are primarily found in certain areas of the midbrain, hypothalamus, and thalamus. Microscopic analysis of LBs reveals fragments of lipid-rich membranes, organelles, and vesicles. These and other pieces of experimental evidence suggest that α-Syn aggregation can be triggered by lipids. In this study, we used atomic force microscope infrared spectroscopy (AFM-IR) to investigate the structural organization of individual α-Syn oligomers grown in the presence of two different phospholipids vesicles. AFM-IR is a modern optical nanoscopy technique that has single-molecule sensitivity and subdiffraction spatial resolution. Our results show that α-Syn oligomers grown in the presence of phosphatidylcholine have a distinctly different structure than oligomers grown in the presence of phosphatidylserine. We infer that this occurs because of specific charges adopted by lipids, which in turn governs protein aggregation. We also found that the protein to phospholipid ratio has a substantial impact on the structure of α-Syn oligomers. These findings demonstrate that α-Syn is far more complex than expected from the perspective of the structural organization of oligomeric species.

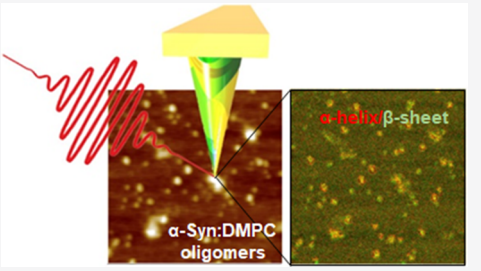

α-Synuclein (α-Syn) is the major component of Lewy bodies (LBs), which are cytoplasmic deposits of proteins in neurons located in several areas of the midbrain, hypothalamus, and thalamus.[1−4] These α-Syn deposits are a pathogenic hallmark of all synucleinopathies, including Parkinson's disease (PD), dementia with Lewy bodies, and multiple-system atrophy.[1,5] Microscopic analysis of LBs revealed the presence of α-Syn fibrils, long unbranched protein aggregates.[6,7] *In vitro* experiments confirmed that α-Syn spontaneously aggregates, first forming small oligomers that later propagate into fibrils.[8−12] The complexity of the cellular environment has a strong effect on shaping α-Syn structure: the difference in condition may lead to different conformations of α-Syn aggregates.[13] There is a growing body of evidence suggesting that oligomers rather than fibrils are responsible for the onset of PD and the spread of DLB in the brain.[14−18] Cryo-electron microscopy (cryo-EM) and solid-state nuclear magnetic resonance (ss-NMR) allowed for the elucidation of the structural organization of α-Syn fibrils.[19−23] However, the transient nature of oligomers and their intrinsic heterogeneity limit cryo-EM and ss-NMR to the structural characterization of these protein aggregates.

Atomic force microscope infrared spectroscopy (AFM-IR) is modern analytical technique that can be used to resolve the secondary structure of individual protein oligomers with subdiffraction spatial resolution.[24−29] Recently reported experimental evidence suggests that AFM-IR can achieve single-monolayer[30] and even single-molecule[31] sensitivity. AFM-IR has been utilized to investigate various topics in biology and surface chemistry including amyloid fibrils,[25,26,32−35] plant epicuticular waxes,[36,37] polymers,[38] malaria blood cells,[39] meteorites,[40] bacteria,[41−43] liposomes,[44] and polycrystalline perovskite films.[45] Our group showed that AFM-IR could be used for the structural characterization of individual α-Syn oligomers.[15] Specifically, we found that α-Syn aggregation in a lipid-free environment yields structurally diverse oligomeric species.[15] Some of them possessed α-helical/unordered structure, whereas others were mostly composed of antiparallel and parallel β-sheets. AFM-IR also revealed the structural rearrangement of antiparallel-to-parallel β-sheet secondary structure upon the proliferation of α-Syn oligomers into fibrils.[15]

Manheim and co-workers recently reported that LBs contain fragments of lipid-rich membranes, organelles, and vesicles.[46,47] Independently, Galvagnion found that the rates of α-Syn aggregation can be significantly altered by lipids as well as the protein-to-lipid ratio (P/L ratio).[48−50] Specifically, it has been shown that an increase in the concentration of 1,2-dimyristoyl-*sn*-glycero-3-phosphatidylserine (DMPS) relative to the

Received: March 13, 2021
Accepted: April 30, 2021

https://doi.org/10.1021/acs.jpclett.1c00820
J. Phys. Chem. Lett. 2021, 12, 4407−4414

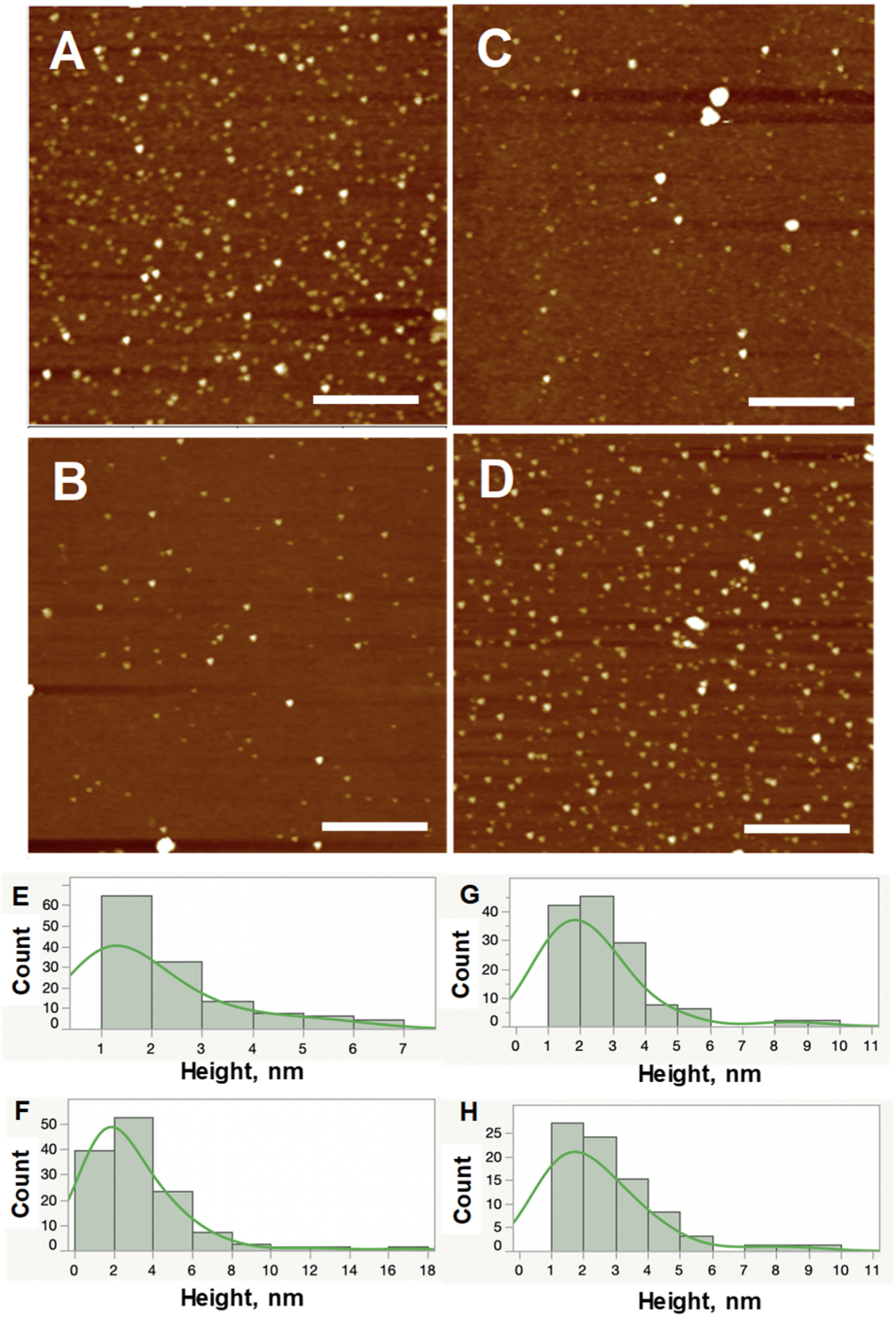

Figure 1. AFM images (A–D) and corresponding height profiles (E–H) of α-Syn-(1:2)-DMPC (A, E), α-Syn-(1:10)-DMPC (B, F), α-Syn-(1:2)-DMPS (C, G), and α-Syn-(1:10)-DMPS (D, H). Scale bars are 1 μm.

concentration of protein first leads to an increase in the rate of α-Syn aggregation. This can be explained from the perspective of lipids as nucleation sites. The larger the number of lipid vesicles, the larger the number of α-Syn aggregation sites and thus faster kinetics of protein aggregation. However, a subsequent increase in the amount of lipids causes a decrease in the kinetics of protein aggregation. This suggests that the delocalization of monomeric α-Syn along surfaces of DMPS vesicles minimizes protein–protein interactions that are necessary for aggregate formation. These experimental findings suggest that phospholipids may not only alter the rates of protein aggregation but also can uniquely modify the secondary structure of α-Syn oligomers.

In this study, we used AFM-IR to investigate the structural organization of individual α-Syn oligomers grown in the presence of 1,2-dimyristoyl-*sn*-glycero-3-phosphocholine (DMPC) (α-Syn-DMPC) in 1:2 (α-Syn-(1:2)-DMPC) and 1:10 (α-Syn-(1:2)-DMPC) ratios. We also utilized AFM-IR to

https://doi.org/10.1021/acs.jpclett.1c00820
J. Phys. Chem. Lett. 2021, 12, 4407–4414

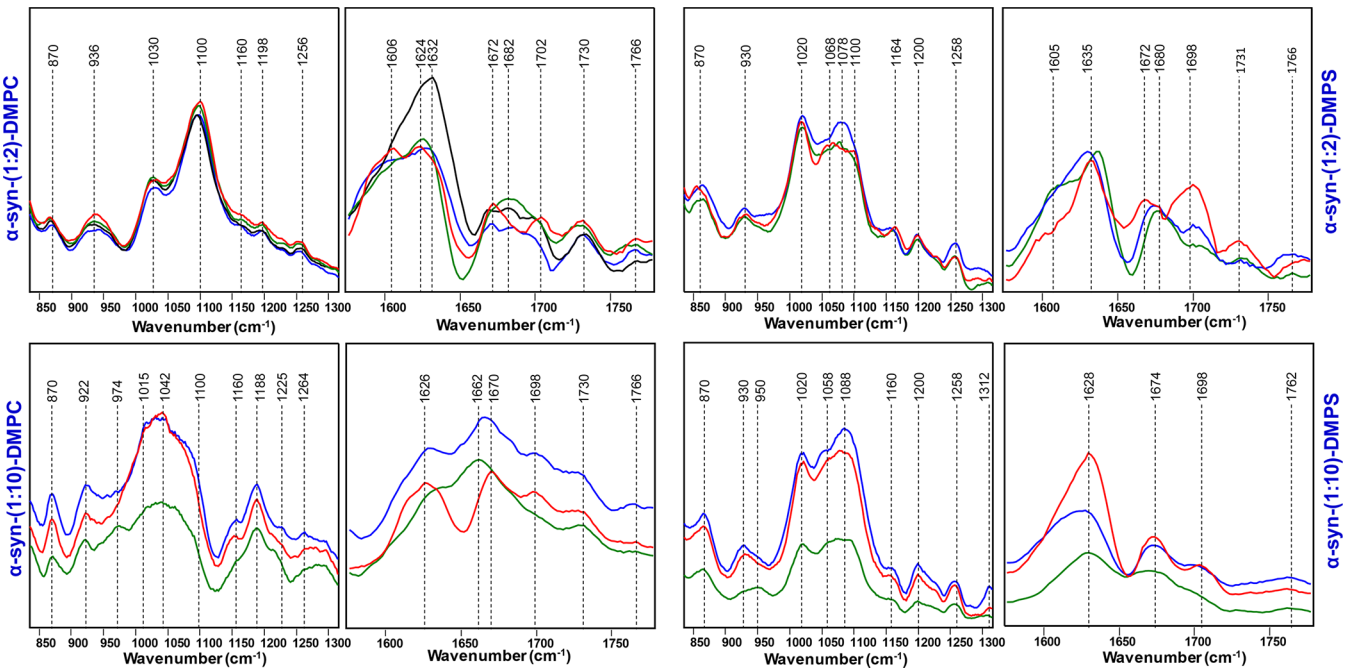

Figure 2. AFM-IR spectra of individual α-Syn-(1:2)-DMPC, α-Syn-(1:10)-DMPC, α-Syn-(1:2)-DMPS, and α-Syn-(1:10)-DMPS oligomers. Blue, red, and green correspond to 1, 2, and 3, and black corresponds to 4 in Figure 3.

probe the structure of α-Syn oligomers grown in the presence of DMPS (α-Syn-DMPS) in 1:2 (α-Syn-(1:2)-DMPS) and 1:10 (α-Syn-(1:2)-DMPS) ratios due to the high abundance of both of these phospholipids in cell and organelle membranes and neurons.[51] Monomeric α-Syn was mixed with large unilamellar vesicles (LUVs) of DMPS (Figures S1 and S2) and DMPC (Figures S3 and S4) in 1:2 and 1:10 ratios; the solutions were kept at room temperature without agitation. On day 2 (D2), an aliquot sample was deposited on a silicon wafer, rinsed with distilled water, and dried immediately under a flow of nitrogen. We found that oligomers in the early stage of α-Syn aggregation had spherical morphology with heights ranging from 1 to 10 nm (Figure 1). Specifically, most of the α-Syn-(1:2)-DMPC and α-Syn-(1:10)-DMPC oligomers were 1−3 and 1−6 nm high, respectively. α-Syn-(1:2)-DMPS and α-Syn-(1:10)-DMPS were 1−4 and 1−5 nm high, respectively. These results suggest that all α-Syn-DMPS and α-Syn-DMPC oligomers exhibit high similarity in both topography and size. It should be noted that we did not observe LUVs upon AFM imaging (Figures S1 and S2). These experimental findings suggest that the formation of α-Syn oligomers is associated with the degradation of LUVs.

AFM-IR analysis of individual α-Syn-(1:2)-DMPC, α-Syn-(1:10)-DMPC, α-Syn-(1:2)-DMPS, and α-Syn-(1:10)-DMPS oligomers revealed major differences in their structural organization (Figure 2 and Figures S5−S8). Specifically, α-Syn-(1:2)-DMPC aggregates exhibited intense vibrational bands at 1624−1632 cm^{-1} which could be assigned to the parallel β-sheet (Table 1). At the same time, vibrational bands at 1672−1682 and 1702 cm^{-1}, which could be assigned to β-turns and antiparallel β-sheets, respectively, had weak intensities. These results show that both the parallel and antiparallel β-sheets as well as β-turns are present in α-Syn-(1:2)-DMPC oligomers.

Our experimental findings suggest that the structural organization of α-Syn-(1:10)-DMPC oligomers is substantially different from that of α-Syn-(1:2)-DMPC oligomers. AFM-IR spectra collected from α-Syn-(1:10)-DMPC oligomers exhibited vibrational bands centered at 1662 and 1670 cm^{-1}, indicating a high content of α-helix/unordered protein secondary structure in these oligomers. We also found vibrational bands at 1626 and 1698 cm^{-1} that demonstrate the presence of both parallel and antiparallel β-sheets in the structure of α-Syn-(1:10)-DMPC oligomers. However, the relative content of these secondary structures is drastically different between α-Syn-(1:2)-DMPC and α-Syn-(1:10)-DMPC oligomers. In α-Syn-(1:2)-DMPC oligomers, the

Table 1. Vibrational Bands and Their Assignments for Phospholipids and Proteins

band wavenumber (cm^{-1})	vibrational mode	assignment
870	C−H	lipid[52,53]
930	ν(C−N^+−C)	lipid (DMPC)[52,53]
920−940	C═C−H	lipid and protein[52,53]
1015−1030	C−O stretch	lipid[54,55]
1030−1050	O···H^+···O stretch or bend	protein[56]
1040−1100	ν(PO_2^-)	lipid[52,54]
1170	ester (C−O) sym stretch	lipid[52]
1160−1200	P═O; C−O−P	lipid[57]
1256−1264	ν(PO_2^-)	lipid[54,58]
1289−1298	N−H	protein[55]
1350	stretching C−O	lipid[59]
1380	CH_3, C−O stretching	lipid[52,58,59]
1460	C−H vibration	lipid and protein
1550	amide II	protein[15]
1610−1640	amide I	β-sheet[15]
1640−1653	amide I	random coil[15]
1648−1660	amide I	α-helix[15]
1660−1685	amide I	3_{10}-helix, type II β-turn[15]
1675−1697	amide I	antiparallel β-sheet[15]
1730−1766	ν(C═O)	lipid[59]

https://doi.org/10.1021/acs.jpclett.1c00820
J. Phys. Chem. Lett. 2021, 12, 4407−4414

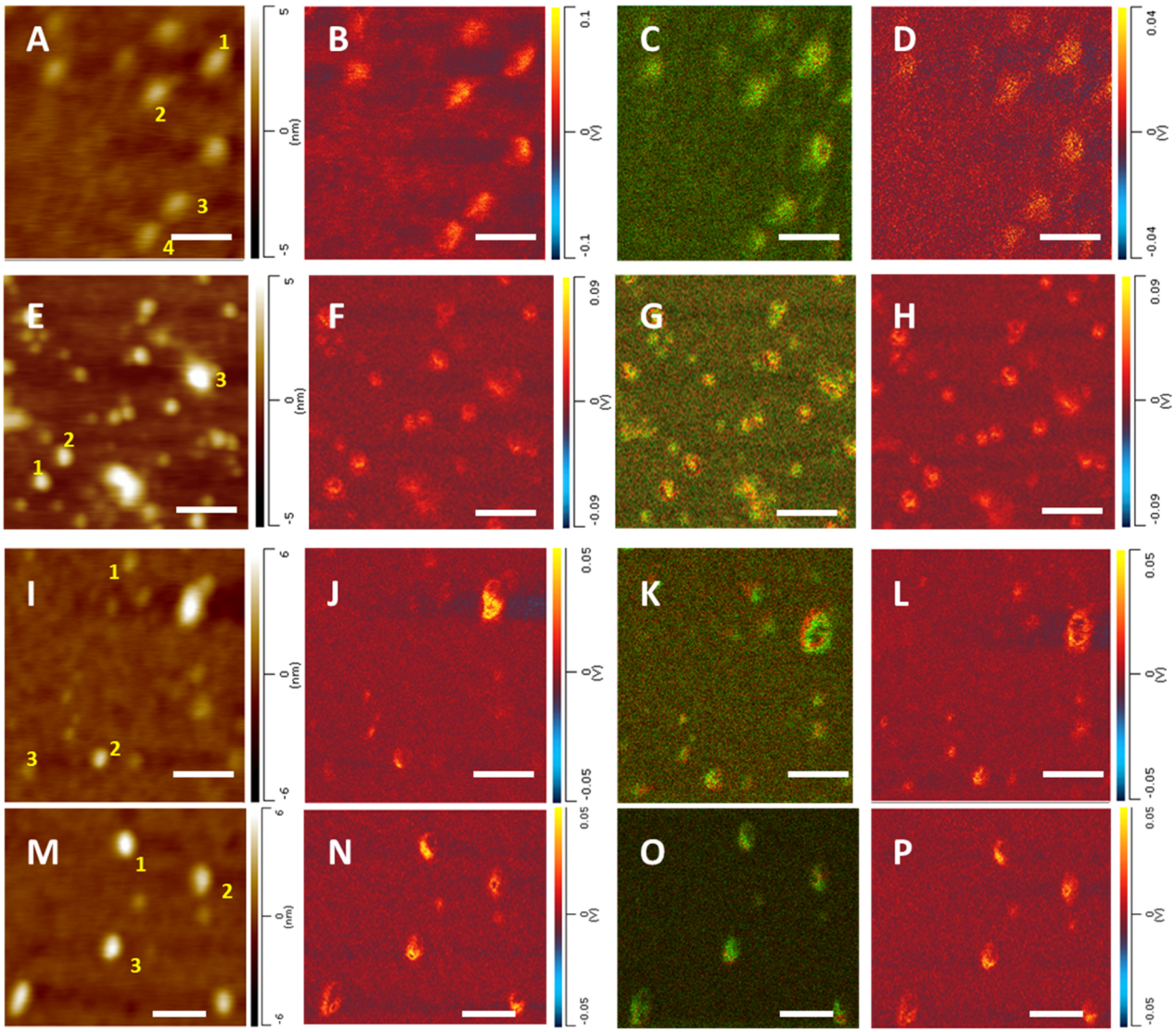

Figure 3. AFM-IR chemical map of α-Syn-(1:2)-DMPC (A–D), α-Syn-(1:10)-DMPC (E–H), α-Syn-(1:2)-DMPS (I–L) and α-Syn-(1:10)-DMPS oligomers (M–P). AFM height images (A, E, I, and M), IR absorption map at 1100 cm^{-1} (ν(PO_2^-) of phospholipids) (B, F, J, N), IR ratio overlaying maps of 1624 cm^{-1} (parallel β-sheet) (green)/1655 cm^{-1} (α-helix/unordered protein secondary structure) (red) (C, G, K, O), and IR absorption map at 1694 cm^{-1} (antiparallel β-sheet) (D, H, L, P). Scale bar, 100 nm.

content in the parallel β-sheet was nearly 3 times higher than that in the unordered and antiparallel β-sheets, whereas in α-Syn-(1:10)-DMPC oligomers the number of α-helix/unordered protein secondary structures was almost twice as high as the number of parallel and antiparallel β-sheets.

AFM-IR spectra of both α-Syn-(1:2)-DMPC and α-Syn-(1:10)-DMPC oligomers exhibited vibrational bands that could be assigned to DMPC (Figure 2 and Figure S4). Specifically, we found a vibrational band at ∼930 cm^{-1} that could be assigned to C–N^+–C vibrations of this phospholipid. We also observed vibrations at 1015–1030 cm^{-1}, which could be assigned to the C–O stretch of the phospholipid and vibrational bands at 1040–1100 cm^{-1} that originate from the phosphor group vibrations. Finally, in the spectra of both α-Syn-(1:2)-DMPC and α-Syn-(1:10)-DMPC, we found a band at 1256–1264 cm^{-1}, which originates from the PO_2^- vibration, as well as vibrational bands at 1730 and 1766 cm^{-1}, which could be assigned to the carbonyl vibration of DMPC. These findings indicate that phospholipid is present in the structures of both α-Syn-(1:2)-DMPC and α-Syn-(1:10)-DMPC. In addition to the change in intensity of the vibrational bands, we found a shift of the PO_2^- vibration in the spectra of α-Syn-(1:2)-DMPC and α-Syn-(1:10)-DMPC. In the spectrum of α-Syn-(1:2)-DMPC, this vibration is centered at 1100 cm^{-1}, whereas in the spectrum of α-Syn-(1:10)-DMPC, this band was found at 1042 cm^{-1}. This blue shift suggests that in the structure of α-Syn-(1:2)-DMPC the charged phosphor group is located in the hydrophilic environment, whereas in α-Syn-(1:10)-DMPC the phosphor group is squeezed into the aqueous environment. Although extensive calculations are required to fully elucidate the conformations of DMPC in both α-Syn-(1:2)-DMPC and α-Syn-(1:10)-DMPC oligomers, one can conclude that this phospholipid has different organizations in those two classes of oligomers.

We also found that α-Syn-(1:10)-DMPC oligomers exhibit very similar if not identical structural organization. This conclusion can be made on the basis of similar profiles of amide I vibrations (1622–1704 cm^{-1}). The higher intensity of the spectrum of one of the oligomers (blue trace) compared to the other three (black, red, and green traces) is likely due to

https://doi.org/10.1021/acs.jpclett.1c00820
J. Phys. Chem. Lett. 2021, 12, 4407–4414

differences in the height of these oligomers. The higher oligomer exhibited a stronger AFM-IR spectrum compared to smaller oligomers. Although α-Syn-(1:2)-DMPC oligomers exhibit similar spectra, their structural heterogeneity is substantially larger. Specifically, we found that one of the examined oligomers (black trace) exhibited a much stronger intensity of 1622−1632 cm^{-1} bands compared to the other three (green, blue, and red). This evidence suggests that this oligomer had a larger number of parallel β-sheets compared to the other oligomers. Also, small changes in the intensities of vibrational bands at 1672−1683 cm^{-1} (β-turns) and 1696−1704 cm^{-1} (antiparallel β-sheet) suggest small deviations in the number of these secondary structural elements in their structure. Thus, α-Syn-(1:2)-DMPC is not as structurally homogeneous as α-Syn-(1:10)-DMPC oligomers.

Spectroscopic analysis of α-Syn-DMPS oligomers revealed the presence of vibrational bands that can be assigned to parallel (1620−1635 cm^{-1}) and antiparallel β-sheet (1694−1696 cm^{-1}) (Figure 2). These spectra also exhibited vibrations at 1672−1680 cm^{-1} that could be assigned to β-turn secondary structure. On the basis of these results, we can conclude that both α-Syn-(1:2)-DMPS and α-Syn-(1:10)-DMPS are primarily composed of parallel and antiparallel β-sheets and β-turns. We also found that α-Syn-(1:2)-DMPS exhibits more heterogeneous content of antiparallel β-sheets compared to α-Syn-(1:10)-DMPS oligomers. Specifically, the heterogeneity arises from different ratios of parallel and antiparallel β-sheets in analyzed oligomers. In two of the analyzed α-Syn-(1:2)-DMPS oligomers, parallel β-sheets prevailed over the content of antiparallel β-sheets. However, in the third oligomer, the numbers of parallel and antiparallel β-sheets were nearly identical.

AFM-IR showed that α-Syn-DMPS oligomers exhibit vibrational bands that could be assigned to DMPS (Table 1, Figure 2, and Figure S2). The vibration at ∼1020 cm^{-1} could be assigned to the C−O stretch, whereas bands from 1070 to 1100 cm^{-1} could be assigned to the phosphate group vibration. Both α-Syn-(1:2)-DMPS and α-Syn-(1:10)-DMPS exhibited high similarity in the lipid region of the spectrum. This suggests similar interaction patterns between α-Syn and DMPS under two different P/L ratios. We also found that a band at ∼1040 cm^{-1}, which was evident in the spectrum of DMPS, shifted to ∼1020 cm^{-1} in the spectra of α-Syn-(1:2)-DMPS and α-Syn-(1:10)-DMPS oligomers. This points out the interactions between polar headgroups of DMPS with α-Syn upon protein aggregation. Extensive density functional theory (DFT) calculations are required to fully elucidate DMPS-α-Syn interactions, which are beyond the scope of the current work.

We observed some heterogeneity within both α-Syn-(1:2)-DMPS and α-Syn-(1:10)-DMPS. α-Syn-(1:2)-DMPS oligomers exhibited heterogeneity related to different ratios of parallel vs antiparallel β-sheets (red vs green and blue curves, α-Syn-(1:2)-DMPS, Figure 2, Figures S7 and S8). The same conclusions can be drawn for α-Syn-(1:10)-DMPS. We found that ratio of parallel vs antiparallel β-sheets (black vs red and blue curves) changes from one oligomer to another. Nevertheless, spectroscopic analysis of both α-Syn-DMPS and α-Syn-DMPC oligomers revealed substantially less structural heterogeneity compared to α-Syn aggregates grown in the lipid-free environment (Figure S9).[15] These findings point out the efficient nucleation of α-Syn aggregation by both DMPS and DMPC.[60] Previously used NMR and fluorescence methods reveal mechanisms of such lipid-templated aggregation of α-Syn. It has been found that zwitterionic headgroups of lipids first interact with lysine and glutamic acid residues on the N-terminus (aa 1−60) of a-syn.[61] Lipid−α-Syn interactions are also enhanced by fatty acids of lipids and the central domain (aa 61−95) of α-Syn, also known as the NAC domain.[62,63] These pieces of experimental evidence demonstrated that the lipid-templated aggregation of α-Syn is driven by both electrostatic and hydrophobic interactions between lipids and proteins.

Next, we performed imaging of these oligomers using AFM-IR. Images were collected at 1100 cm^{-1} (phospholipids), 1624 cm^{-1} (parallel β-sheet), 1655 cm^{-1} (α-helix/unordered protein secondary structure), and 1694 cm^{-1} (antiparallel β-sheet) to probe the localization of lipids and protein secondary structure elements in the structure of all four types of oligomers (Figure 3).

We found that both phospholipids are homogeneously distributed in α-Syn-(1:2)-DMPC, α-Syn-(1:10)-DMPC, α-Syn-(1:2)-DMPS, and α-Syn-(1:10)-DMPS. AFM-IR imaging confirmed the above-discussed ratio of parallel-to-antiparallel β-sheets in α-Syn-(1:2)-DMPC and α-Syn-(1:10)-DMPC. Specifically, α-Syn-(1:10)-DMPC exhibits very similar ratios of parallel and antiparallel β-sheets in their structures (Figure 3F,H), whereas the parallel β-sheet dominates in the structure of α-Syn-(1:2)-DMPC. We also found that α-Syn-(1:2)-DMPC is nearly entirely composed of parallel β-sheets (Figure 3C), whereas a substantial amount of α-helix has been observed in α-Syn-(1:10)-DMPC (Figure 3G). α-Syn-(1:2)-DMPS and α-Syn-(1:10)-DMPS exhibited primarily parallel β-sheet secondary structure, with detectable α-helix content at the edges of the oligomers.

A growing body of evidence points to a direct relationship between the crude shape of α-Syn oligomers and their propensity for exerting toxicity.[64−67] Specifically, it has been found that small annular α-Syn oligomers induce Ca^{2+} influx, caspase activation, and cell death, whereas larger α-Syn oligomers exhibit no toxicity.[65] These findings suggest that oligomer toxicity is likely to be determined by their structure.[68] Although the exact mechanisms by which oligomers exert their toxicity are unclear, it has been proposed that endocytosed α-Syn aggregates can impair lysosomal activity and suppress autophagosome clearance.[69,70] Alternatively, amyloid oligomers can disrupt the integrity of cell and mitochondrial membranes, causing cell death.[14,29,71] One can expect that the presence of lipids in the structure of α-Syn oligomers grown in the presence of DMPC and DMPS can significantly alter oligomer−membrane interactions. This can lead to a decrease or an increase in cell toxicity.

In summary, our findings demonstrate that α-Syn oligomers grown in the presence of DMPC and DMPS have significantly different secondary structures compared to α-Syn oligomers grown in a lipid-free environment. Furthermore, both phospholipids are present in the structure of the α-Syn-DMPC and α-Syn-DMPS oligomers. We also found that α-Syn-DMPC oligomers are drastically different from α-Syn-DMPS aggregates in terms of their secondary structure. Finally, we found that not only the chemical structure of the lipid but also the P/L ratio alters the secondary structure of α-Syn oligomers. This detail biophysical characterization of α-Syn aggregates grown in the presence of two phospholipids sets the foundation for the elucidation of the toxicity of these aggregates *in vivo* and *in vitro*.

https://doi.org/10.1021/acs.jpclett.1c00820
J. Phys. Chem. Lett. 2021, 12, 4407−4414

■ ASSOCIATED CONTENT

Supporting Information

The Supporting Information is available free of charge at https://pubs.acs.org/doi/10.1021/acs.jpclett.1c00820.

Detailed description of sample preparation, spectra acquisition methods, and instrumentation (PDF)

■ AUTHOR INFORMATION

Corresponding Author

Dmitry Kurouski − *Department of Biochemistry and Biophysics and The Institute for Quantum Science and Engineering, Texas A&M University, College Station, Texas 77843, United States;* orcid.org/0000-0002-6040-4213; Phone: 979-458-3778; Email: dkurouski@tamu.edu

Authors

Tianyi Dou − *Department of Biochemistry and Biophysics, Texas A&M University, College Station, Texas 77843, United States*

Lei Zhou − *The Institute for Quantum Science and Engineering, Texas A&M University, College Station, Texas 77843, United States*

Complete contact information is available at: https://pubs.acs.org/10.1021/acs.jpclett.1c00820

Author Contributions

L.Z. and D.K. designed the research. T.D. and L.Z. conducted AFM-IR experiments, T.D. analyzed the data. D.K. wrote the article with input from T.D.

Notes

The authors declare no competing financial interest.

■ ACKNOWLEDGMENTS

We are grateful to AgriLife Research of Texas A&M for financial support. We also acknowledge the Governor's University Research Initiative (GURI) grant program of Texas A&M University (GURI grant agreement no. 12-2016, M1700437). This work was supported by start-up funds from Texas A&M University.

■ REFERENCES

(1) Surmeier, D. J.; Obeso, J. A.; Halliday, G. M. Selective Neuronal Vulnerability in Parkinson Disease. *Nat. Rev. Neurosci.* **2017**, *18*, 101−113.

(2) Goedert, M.; Spillantini, M. G.; Del Tredici, K.; Braak, H. 100 Years of Lewy Pathology. *Nat. Rev. Neurol.* **2013**, *9*, 13−24.

(3) Braak, H.; Ghebremedhin, E.; Rub, U.; Bratzke, H.; Del Tredici, K. Stages in the Development of Parkinson's Disease-Related Pathology. *Cell Tissue Res.* **2004**, *318*, 121−34.

(4) Del Tredici, K.; Rub, U.; De Vos, R. A.; Bohl, J. R.; Braak, H. Where Does Parkinson Disease Pathology Begin in the Brain? *J. Neuropathol. Exp. Neurol.* **2002**, *61*, 413−26.

(5) Hawkes, C. H.; Del Tredici, K.; Braak, H. Parkinson's Disease: A Dual-Hit Hypothesis. *Neuropathol. Appl. Neurobiol.* **2007**, *33*, 599−614.

(6) Mahul-Mellier, A. L.; Burtscher, J.; Maharjan, N.; Weerens, L.; Croisier, M.; Kuttler, F.; Leleu, M.; Knott, G. W.; Lashuel, H. A. The Process of Lewy Body Formation, Rather Than Simply Alpha-Synuclein Fibrillization, Is One of the Major Drivers of Neurodegeneration. *Proc. Natl. Acad. Sci. U. S. A.* **2020**, *117*, 4971−4982.

(7) Forno, L. S.; DeLanney, L. E.; Irwin, I.; Langston, J. W. Electron Microscopy of Lewy Bodies in the Amygdala-Parahippocampal Region. Comparison with Inclusion Bodies in the Mptp-Treated Squirrel Monkey. *Adv. Neurol.* **1996**, *69*, 217−228.

(8) Fares, M. B.; Maco, B.; Oueslati, A.; Rockenstein, E.; Ninkina, N.; Buchman, V. L.; Masliah, E.; Lashuel, H. A. Induction of De Novo Alpha-Synuclein Fibrillization in a Neuronal Model for Parkinson's Disease. *Proc. Natl. Acad. Sci. U. S. A.* **2016**, *113*, E912−21.

(9) Bodner, R. A.; Outeiro, T. F.; Altmann, S.; Maxwell, M. M.; Cho, S. H.; Hyman, B. T.; McLean, P. J.; Young, A. B.; Housman, D. E.; Kazantsev, A. G. Pharmacological Promotion of Inclusion Formation: A Therapeutic Approach for Huntington's and Parkinson's Diseases. *Proc. Natl. Acad. Sci. U. S. A.* **2006**, *103*, 4246−51.

(10) Chen, M.; Margittai, M.; Chen, J.; Langen, R. Investigation of Alpha-Synuclein Fibril Structure by Site-Directed Spin Labeling. *J. Biol. Chem.* **2007**, *282*, 24970−9.

(11) Conway, K. A.; Harper, J. D.; Lansbury, P. T. Accelerated in Vitro Fibril Formation by a Mutant Alpha-Synuclein Linked to Early-Onset Parkinson Disease. *Nat. Med.* **1998**, *4*, 1318−20.

(12) Crowther, R. A.; Daniel, S. E.; Goedert, M. Characterisation of Isolated Alpha-Synuclein Filaments from Substantia Nigra of Parkinson's Disease Brain. *Neurosci. Lett.* **2000**, *292*, 128−30.

(13) Stephens, A. D.; Zacharopoulou, M.; Kaminski Schierle, G. S. The Cellular Environment Affects Monomeric A-Synuclein Structure. *Trends Biochem. Sci.* **2019**, *44*, 453−466.

(14) Winner, B.; et al. In Vivo Demonstration That -Synuclein Oligomers Are Toxic. *Proc. Natl. Acad. Sci. U. S. A.* **2011**, *108*, 4194−4199.

(15) Zhou, L.; Kurouski, D. Structural Characterization of Individual Alpha-Synuclein Oligomers Formed at Different Stages of Protein Aggregation by Atomic Force Microscopy-Infrared Spectroscopy. *Anal. Chem.* **2020**, *92*, 6806−6810.

(16) Hoyer, W.; Antony, T.; Cherny, D.; Heim, G.; Jovin, T. M.; Subramaniam, V. Dependence of Alpha-Synuclein Aggregate Morphology on Solution Conditions. *J. Mol. Biol.* **2002**, *322*, 383−93.

(17) Qin, Z.; Hu, D.; Han, S.; Hong, D. P.; Fink, A. L. Role of Different Regions of Alpha-Synuclein in the Assembly of Fibrils. *Biochemistry* **2007**, *46*, 13322−30.

(18) Vilar, M.; Chou, H. T.; Luhrs, T.; Maji, S. K.; Riek-Loher, D.; Verel, R.; Manning, G.; Stahlberg, H.; Riek, R. The Fold of Alpha-Synuclein Fibrils. *Proc. Natl. Acad. Sci. U. S. A.* **2008**, *105*, 8637−42.

(19) Schweighauser, M.; et al. Structures of A-Synuclein Filaments from Multiple System Atrophy. *Nature* **2020**, *585*, 464−469.

(20) Strohäker, T.; et al. Structural Heterogeneity of A-Synuclein Fibrils Amplified from Patient Brain Extracts. *Nat. Commun.* **2019**, *10*, 5535.

(21) Li, B.; et al. Cryo-Em of Full-Length A-Synuclein Reveals Fibril Polymorphs with a Common Structural Kernel. *Nat. Commun.* **2018**, *9*, 3609.

(22) Paravastu, A. K.; Petkova, A. T.; Tycko, R. Polymorphic Fibril Formation by Residues 10−40 of the Alzheimer's Beta-Amyloid Peptide. *Biophys. J.* **2006**, *90*, 4618−29.

(23) Paravastu, A. K.; Qahwash, I.; Leapman, R. D.; Meredith, S. C.; Tycko, R. Seeded Growth of Beta-Amyloid Fibrils from Alzheimer's Brain-Derived Fibrils Produces a Distinct Fibril Structure. *Proc. Natl. Acad. Sci. U. S. A.* **2009**, *106*, 7443−8.

(24) Kurouski, D.; Dazzi, A.; Zenobi, R.; Centrone, A. Infrared and Raman Chemical Imaging and Spectroscopy at the Nanoscale. *Chem. Soc. Rev.* **2020**, *49*, 3315−3347.

(25) Ruggeri, F. S.; Longo, G.; Faggiano, S.; Lipiec, E.; Pastore, A.; Dietler, G. Infrared Nanospectroscopy Characterization of Oligomeric and Fibrillar Aggregates During Amyloid Formation. *Nat. Commun.* **2015**, *6*, 7831.

(26) Ruggeri, F. S.; Vieweg, S.; Cendrowska, U.; Longo, G.; Chiki, A.; Lashuel, H. A.; Dietler, G. Nanoscale Studies Link Amyloid Maturity with Polyglutamine Diseases Onset. *Sci. Rep.* **2016**, *6*, 31155.

(27) Centrone, A. Infrared Imaging and Spectroscopy Beyond the Diffraction Limit. *Annu. Rev. Anal. Chem.* **2015**, *8*, 101−126.

(28) Dazzi, A.; Prater, C. B. Afm-Ir: Technology and Applications in Nanoscale Infrared Spectroscopy and Chemical Imaging. *Chem. Rev.* **2017**, *117*, 5146−5173.

(29) Chen, S. W.; et al. Structural Characterization of Toxic Oligomers That Are Kinetically Trapped During Alpha-Synuclein

Fibril Formation. *Proc. Natl. Acad. Sci. U. S. A.* **2015**, *112*, E1994−2003.
(30) Lu, F.; Jin, M. Z.; Belkin, M. A. Tip-Enhanced Infrared Nanospectroscopy Via Molecular Expansion Force Detection. *Nat. Photonics* **2014**, *8*, 307−312.
(31) Ruggeri, F. S.; Mannini, B.; Schmid, R.; Vendruscolo, M.; Knowles, T. P. J. Single Molecule Secondary Structure Determination of Proteins through Infrared Absorption Nanospectroscopy. *Nat. Commun.* **2020**, *11*, 2945.
(32) Ruggeri, F. S.; Benedetti, F.; Knowles, T. P. J.; Lashuel, H. A.; Sekatskii, S.; Dietler, G. Identification and Nanomechanical Characterization of the Fundamental Single-Strand Protofilaments of Amyloid Alpha-Synuclein Fibrils. *Proc. Natl. Acad. Sci. U. S. A.* **2018**, *115*, 7230−7235.
(33) Ruggeri, F. S.; Flagmeier, P.; Kumita, J. R.; Meisl, G.; Chirgadze, D. Y.; Bongiovanni, M. N.; Knowles, T. P. J.; Dobson, C. M. The Influence of Pathogenic Mutations in Alpha-Synuclein on Biophysical and Structural Characteristics of Amyloid Fibrils. *ACS Nano* **2020**, *14*, 5213−5222.
(34) Rizevsky, S.; Kurouski, D. Nanoscale Structural Organization of Insulin Fibril Polymorphs Revealed by Atomic Force Microscopy-Infrared Spectroscopy (AFM-IR). *ChemBioChem* **2020**, *21*, 481−485.
(35) Ramer, G.; Ruggeri, F. S.; Levin, A.; Knowles, T. P. J.; Centrone, A. Determination of Polypeptide Conformation with Nanoscale Resolution in Water. *ACS Nano* **2018**, *12*, 6612−6619.
(36) Farber, C.; Li, J.; Hager, E.; Chemelewski, R.; Mullet, J.; Rogachev, A. Y.; Kurouski, D. Complementarity of Raman and Infrared Spectroscopy for Structural Characterization of Plant Epicuticular Waxes. *ACS Omega* **2019**, *4*, 3700−3707.
(37) Farber, C.; Wang, R.; Chemelewski, R.; Mullet, J.; Kurouski, D. Nanoscale Structural Organization of Plant Epicuticular Wax Probed by Atomic Force Microscope Infrared Spectroscopy. *Anal. Chem.* **2019**, *91*, 2472−2479.
(38) Dazzi, A. Photothermal Induced Resonance: Application to Infrared Spectromicroscopy. In *Thermal Nanosystems and Nanomaterials*; Volz, S., Ed.; Springer: Berlin, 2009; Vol. *118*, pp 469−503.
(39) Perez-Guaita, D.; Kochan, K.; Batty, M.; Doerig, C.; Garcia-Bustos, J.; Espinoza, S.; McNaughton, D.; Heraud, P.; Wood, B. R. Multispectral Atomic Force Microscopy-Infrared Nano-Imaging of Malaria Infected Red Blood Cells. *Anal. Chem.* **2018**, *90*, 3140−3148.
(40) Mathurin, J.; Dartois, E.; Pino, T.; Engrand, C.; Duprat, J.; Deniset-Besseau, A.; Borodnics, F.; Sandt, C.; Dazzi, A. Nanometer Scale Infrared Chemical Imaging of Organic Matter in Ultracarbonaceous Antarctic Micrometeorites (Ucamm). *Astron. Astrophys.* **2019**, *622*, A160.
(41) Dazzi, A.; Prazeres, R.; Glotin, F.; Ortega, J. M.; Al-Sawaftah, M.; de Frutos, M. Chemical Mapping of the Distribution of Viruses into Infected Bacteria with a Photothermal Method. *Ultramicroscopy* **2008**, *108*, 635−641.
(42) Mayet, C.; Deniset-Besseau, A.; Prazeres, R.; Ortega, J. M.; Dazzi, A. Analysis of Bacterial Polyhydroxybutyrate Production by Multimodal Nanoimaging. *Biotechnol. Adv.* **2013**, *31*, 369−374.
(43) Kochan, K.; Perez-Guaita, D.; Pissang, J.; Jiang, J. H.; Peleg, A. Y.; McNaughton, D.; Heraud, P.; Wood, B. R. In Vivo Atomic Force Microscopy-Infrared Spectroscopy of Bacteria. *J. R. Soc., Interface* **2018**, *15*, 20180115.
(44) Wieland, K.; Ramer, G.; Weiss, V. U.; Allmaier, G.; Lendl, B.; Centrone, A. Nanoscale Chemical Imaging of Individual Chemotherapeutic Cytarabine-Loaded Liposomal Nanocarriers. *Nano Res.* **2019**, *12*, 197−203.
(45) Strelcov, E.; Dong, Q.; Li, T.; Chae, J.; Shao, Y.; Deng, Y.; Gruverman, A.; Huang, J.; Centrone, A. Ch3nh3pbi3 Perovskites: Ferroelasticity Revealed. *Sci. Adv.* **2017**, *3*, No. e1602165.
(46) Shahmoradian, S. H.; et al. Lewy Pathology in Parkinson's Disease Consists of Crowded Organelles and Lipid Membranes. *Nat. Neurosci.* **2019**, *22*, 1099−1109.
(47) Killinger, B. A.; Melki, R.; Brundin, P.; Kordower, J. H. Endogenous Alpha-Synuclein Monomers, Oligomers and Resulting Pathology: Let's Talk About the Lipids in the Room. *N.P.J. Parkinsons Dis.* **2019**, *5*, 23.
(48) Alza, N. P.; Iglesias Gonzalez, P. A.; Conde, M. A.; Uranga, R. M.; Salvador, G. A. Lipids at the Crossroad of Alpha-Synuclein Function and Dysfunction: Biological and Pathological Implications. *Front. Cell. Neurosci.* **2019**, *13*, 175.
(49) Galvagnion, C. The Role of Lipids Interacting with -Synuclein in the Pathogenesis of Parkinson's Disease. *J. Parkinson's Dis.* **2017**, *7*, 433−450.
(50) Galvagnion, C.; Brown, J. W.; Ouberai, M. M.; Flagmeier, P.; Vendruscolo, M.; Buell, A. K.; Sparr, E.; Dobson, C. M. Chemical Properties of Lipids Strongly Affect the Kinetics of the Membrane-Induced Aggregation of Alpha-Synuclein. *Proc. Natl. Acad. Sci. U. S. A.* **2016**, *113*, 7065−70.
(51) Fitzner, D.; Bader, J. M.; Penkert, H.; Bergner, C. G.; Su, M.; Weil, M. T.; Surma, M. A.; Mann, M.; Klose, C.; Simons, M. Cell-Type- and Brain-Region-Resolved Mouse Brain Lipidome. *Cell Rep.* **2020**, *32*, 108132.
(52) Blume, A. Properties of Lipid Vesicles: Ft-Ir Spectroscopy and Fluorescence Probe Studies. *Curr. Opin. Colloid Interface Sci.* **1996**, *1*, 64−77.
(53) Cagnasso, M.; Boero, V.; Franchini, M. A.; Chorover, J. Atr-Ftir Studies of Phospholipid Vesicle Interactions with A-Feooh and A-Fe2o3 Surfaces. *Colloids Surf., B* **2010**, *76*, 456−467.
(54) Wood, B. R.; Quinn, M. A.; Tait, B.; Ashdown, M.; Hislop, T.; Romeo, M.; McNaughton, D. Ftir Microspectroscopic Study of Cell Types and Potential Confounding Variables in Screening for Cervical Malignancies. *Biospectroscopy* **1998**, *4*, 75−91.
(55) Wood, B. R.; Quinn, M. A.; Burden, F. R.; McNaughton, D. An Investigation into Ftir Spectroscopy as a Biodiagnostic Tool for Cervical Cancer. *Biospectroscopy* **1996**, *2*, 143−153.
(56) Barth, A. Infrared Spectroscopy of Proteins. *Biochim. Biophys. Acta, Bioenerg.* **2007**, *1767*, 1073−1101.
(57) Yoshida, S.; Miyazaki, M.; Sakai, K.; Takeshita, M.; Yuasa, S.; Sato, A.; Kobayashi, T.; Watanabe, S.; Okuyama, H. Fourier Transform Infrared Spectroscopic Analysis of Rat Brain Microsomal Membranes Modified by Dietary Fatty Acids: Possible Correlation with Altered Learning Behavior. *Biospectroscopy* **1997**, *3*, 281−290.
(58) Richter, T.; Steiner, G.; Abu-Id, M. H.; Salzer, R.; Bergmann, R.; Rodig, H.; Johannsen, B. Identification of Tumor Tissue by Ftir Spectroscopy in Combination with Positron Emission Tomography. *Vib. Spectrosc.* **2002**, *28*, 103−110.
(59) Movasaghi, Z.; Rehman, S.; Ur Rehman, D. I. Fourier Transform Infrared (Ftir) Spectroscopy of Biological Tissues. *Appl. Spectrosc. Rev.* **2008**, *43*, 134−179.
(60) Galvagnion, C. The Role of Lipids Interacting with A-Synuclein in the Pathogenesis of Parkinson's Disease. *J. Parkinson's Dis.* **2017**, *7*, 433−450.
(61) Viennet, T.; et al. Structural Insights from Lipid-Bilayer Nanodiscs Link Alpha-Synuclein Membrane-Binding Modes to Amyloid Fibril Formation. *Commun. Biol.* **2018**, *1*, 44.
(62) Giasson, B. I.; Murray, I. V.; Trojanowski, J. Q.; Lee, V. M. A Hydrophobic Stretch of 12 Amino Acid Residues in the Middle of Alpha-Synuclein Is Essential for Filament Assembly. *J. Biol. Chem.* **2001**, *276*, 2380−6.
(63) Ueda, K.; Fukushima, H.; Masliah, E.; Xia, Y.; Iwai, A.; Yoshimoto, M.; Otero, D. A.; Kondo, J.; Ihara, Y.; Saitoh, T. Molecular Cloning of Cdna Encoding an Unrecognized Component of Amyloid in Alzheimer Disease. *Proc. Natl. Acad. Sci. U. S. A.* **1993**, *90*, 11282−6.
(64) Chen, L.; Jin, J.; Davis, J.; Zhou, Y.; Wang, Y.; Liu, J.; Lockhart, P. J.; Zhang, J. Oligomeric Alpha-Synuclein Inhibits Tubulin Polymerization. *Biochem. Biophys. Res. Commun.* **2007**, *356*, 548−53.
(65) Danzer, K. M.; Haasen, D.; Karow, A. R.; Moussaud, S.; Habeck, M.; Giese, A.; Kretzschmar, H.; Hengerer, B.; Kostka, M. Different Species of Alpha-Synuclein Oligomers Induce Calcium Influx and Seeding. *J. Neurosci.* **2007**, *27*, 9220−32.
(66) Nasstrom, T.; Fagerqvist, T.; Barbu, M.; Karlsson, M.; Nikolajeff, F.; Kasrayan, A.; Ekberg, M.; Lannfelt, L.; Ingelsson, M.;

https://doi.org/10.1021/acs.jpclett.1c00820
J. Phys. Chem. Lett. 2021, 12, 4407−4414

Bergstrom, J. The Lipid Peroxidation Products 4-Oxo-2-Nonenal and 4-Hydroxy-2-Nonenal Promote the Formation of Alpha-Synuclein Oligomers with Distinct Biochemical, Morphological, and Functional Properties. *Free Radical Biol. Med.* **2011**, *50*, 428−37.
(67) Sharon, R.; Bar-Joseph, I.; Frosch, M. P.; Walsh, D. M.; Hamilton, J. A.; Selkoe, D. J. The Formation of Highly Soluble Oligomers of Alpha-Synuclein Is Regulated by Fatty Acids and Enhanced in Parkinson's Disease. *Neuron* **2003**, *37*, 583−95.
(68) Danzer, K. M.; Haasen, D.; Karow, A. R.; Moussaud, S.; Habeck, M.; Giese, A.; Kretzschmar, H.; Hengerer, B.; Kostka, M. Different Species of -Synuclein Oligomers Induce Calcium Influx and Seeding. *J. Neurosci.* **2007**, *27*, 9220−9232.
(69) Hoffmann, A. C.; et al. Extracellular Aggregated Alpha Synuclein Primarily Triggers Lysosomal Dysfunction in Neural Cells Prevented by Trehalose. *Sci. Rep.* **2019**, *9*, 544.
(70) Vogiatzi, T.; Xilouri, M.; Vekrellis, K.; Stefanis, L. Wild Type Alpha-Synuclein Is Degraded by Chaperone-Mediated Autophagy and Macroautophagy in Neuronal Cells. *J. Biol. Chem.* **2008**, *283*, 23542−23556.
(71) Srinivasan, S.; et al. Pathogenic Serum Amyloid a 1.1 Shows a Long Oligomer-Rich Fibrillation Lag Phase Contrary to the Highly Amyloidogenic Non-Pathogenic Saa2.2. *J. Biol. Chem.* **2013**, *288*, 2744−55.

https://doi.org/10.1021/acs.jpclett.1c00820
J. Phys. Chem. Lett. 2021, 12, 4407−4414